Journal of Marine Research, 54, 1179–1205, 1996

A key role for iron-bound phosphorus in authigenic apatite formation in North Atlantic continental platform sediments

by Caroline P. Slomp[1,2], Eric H. G. Epping[1,3], Willem Helder[1], and Wim Van Raaphorst[1]

ABSTRACT

A combination of pore water and solid phase analysis was used to determine whether authigenic carbonate fluorapatite (CFA) is currently forming in the sediment at two locations (OMEX I and II) on the North Atlantic continental platform Goban Spur (southwest of Ireland). Results of selective P extractions suggest that an early diagenetic redistribution of Fe-bound P to an authigenic P phase may be occurring at both stations. A steady-state diagenetic model describing the depth profiles of pore water HPO_4^{2-} and three solid phase forms of P (organic P, Fe-bound P and authigenic P) was developed and applied to the data of station OMEX-I. The model results indicate that CFA formation can account for the observed increase of authigenic P with depth at this station. Furthermore, the results show that an intense cycling of P between Fe-bound P and pore water HPO_4^{2-} at the redox interface can create conditions beneficial for CFA formation. This internal P cycle is driven by downward, bioturbational transport of mainly *in-situ*-formed Fe-bound P into the reduced sediment zone. Losses from the internal P cycle due to CFA formation and HPO_4^{2-} diffusion are compensated for by sorption of HPO_4^{2-} released from organic matter to Fe oxides in the oxidized surface sediment. Fe-bound P thus acts as an intermediate between organic P and CFA. CFA can account for between 25 and 70% of the total burial flux of reactive P at station OMEX-I and thus may act as an important sink for P in this low sedimentation, continental margin environment.

1. Introduction

Phosphorus (P) is an essential nutrient for marine phytoplankton and has been suggested as the limiting factor for oceanic primary production on geological timescales (Howarth *et al.,* 1995). As sediments form the only important sink for P in the marine environment, changes in the burial rate of P in sediments can modify the oceanic inventory of P and thus profoundly influence marine carbon cycling (Broecker and Peng, 1982). Most removal of P from the water column takes place through sedimentation of organic matter (Berner *et al.,* 1993). Consequently, it is of prime importance to know the fate of the P in organic matter upon reaching the sediment.

1. Netherlands Institute for Sea Research (NIOZ). P.O. Box 59, 1790 AB Den Burg, Texel, The Netherlands.
2. Corresponding author. present address: Department of Phytopathology, Wageningen Agricultural University, P.O. Box 8025, 6700 EE Wageningen, The Netherlands.
3. Present address: Max Planck Institute for Marine Microbiology, Celsiusstr. 1, D-28359 Bremen, Germany.

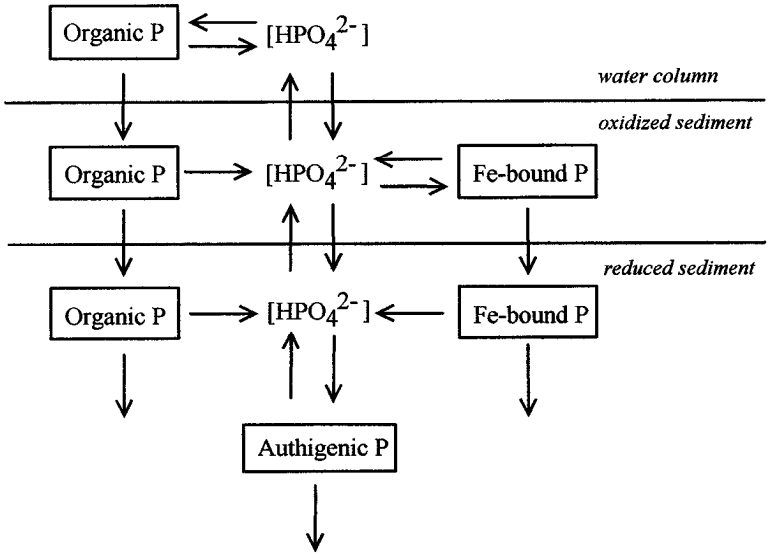

Figure 1. A schematic overview of the sedimentary P cycle. Note that in this view, biogenic Ca-P, $CaCO_3$- and clay-bound P and detrital Ca-P are assumed to be unimportant as a source or sink for dissolved reactive phosphorus.

As shown in the schematic overview of the sedimentary P cycle in Figure 1, part of the P in organic matter is buried directly as organic P. The nonrefractory portion of the organic matter decomposes, however, resulting in a release of HPO_4^{2-} to the pore water. In the oxidized part of the sediment, this HPO_4^{2-} escapes to the overlying water through upward diffusion or is sorbed, either reversibly or irreversibly, to sediment Fe oxides (e.g. Sundby *et al.,* 1992; Slomp *et al.,* 1996). In the reduced sediment zone HPO_4^{2-} is not only released from organic matter but also due to the reduction of Fe oxides. In this part of the sediment, dissolved HPO_4^{2-} concentrations can become high enough for authigenic mineral formation to occur (e.g. Van Cappellen and Berner, 1988). Whether this actually takes place is important, as P bound in authigenic minerals may not be solubilized again, whereas Fe-bound and organic P can still be released upon deep burial.

Evidence for authigenic mineral formation in marine sediments outside classical phosphorite accumulation environments in upwelling areas (e.g. the Peru continental margin; Froelich *et al.,* 1988) is difficult to obtain. Due to the low concentrations of authigenic P, direct identification (e.g. with X-ray diffraction) is often impossible. This makes it necessary to rely on indirect methods. These include calculation of the saturation state of the pore water with respect to authigenic P minerals (Martens *et al.,* 1978; Jahnke *et al.,* 1983), the use of stoichiometric models describing NH_4^+ and HPO_4^{2-} regeneration to detect a possible deficit of HPO_4^{2-} with respect to NH_4^+ (Martens *et al.,* 1978), and application of selective extraction procedures (Ruttenberg, 1992).

Using all of these methods, Ruttenberg and Berner (1993) showed that authigenic

carbonate fluorapatite (CFA) formation is occurring in rapidly accumulating continental margin sediments dominated by terrigenous material. Based on mirror-image profiles of organic and authigenic P, they concluded that at their two study sites HPO_4^{2-} released from organic material is almost completely retained in the sediment due to an early diagenetic 'sink-switching' to CFA. Using the same selective extraction procedure for authigenic P, Lucotte *et al.* (1994) showed that P retention due to CFA formation may also occur in continental rise sediments. In this case, however, Fe-bound P acted as the major source of P and the overall CFA precipitation rate was much lower.

We expect Fe-bound P to play a key role in CFA formation in many marine sediments for two reasons. Firstly, Fe-bound P can act as an intermediate between organic P and CFA. Dissolved HPO_4^{2-} released from labile organic matter, that otherwise would rapidly escape to the overlying water, is retained in the sediment. This HPO_4^{2-} can then cycle between the dissolved and Fe-bound P pool many times, before being permanently bound in CFA. Secondly, HPO_4^{2-} release from Fe oxides has been observed to be accompanied by a simultaneous release of fluoride. The resulting spike of both solutes may provide the condition of supersaturation required for the precipitation of CFA (Heggie *et al.,* 1990; Ruttenberg and Berner, 1993).

In this study, we apply the extraction procedure for authigenic P developed by Ruttenberg (1992) to sediments from two low sedimentation environments on a North Atlantic continental platform. These results are combined with pore water and solid phase data to determine whether CFA formation is an early diagenetic event in these sediments, and if so, whether there is evidence for a key role of Fe-bound P in CFA formation. A diagenetic model for the sedimentary P cycle is developed and applied to the data to facilitate interpretation of the observed depth profiles.

2. Study sites

Two locations on the continental platform Goban Spur, which is situated in the North Atlantic Ocean, southwest of Ireland (Fig. 2), were selected for this study. This broad platform (200–2000 m water depth) is connected to the Celtic Sea continental shelf in the east, is incised by deep canyons on its southern side, whereas to the north and west, the platform slopes down into the Porcupine Basin and the Porcupine Abyssal Plain, respectively. Sediment trap and current meter deployments show that the platform is a biologically and physically dynamic environment, dominated by lateral particle transport and high current velocities (Antia and Von Bodungen, in prep.). Samples were collected during an OMEX (Ocean Margin Exchange) cruise with RV *Pelagia* in October 1993. Station OMEX-I (49°24.72′N, 11°31.86′W) is located on the eastern, relatively shallow part of the platform (at a water depth of 670 m), whereas station OMEX-II (49°11.20′N, 12°49.18′W) is located on the deeper, western part of the platform (at a water depth of 1425 m).

Bottom water temperature was higher at station I (10°C) than at the deeper station II (5.9°C). Holocene sediment accumulation rates of 0.0025 and 0.0011 cm y^{-1} were estimated for stations I and II, respectively, using planktonic foraminiferal biostratigraphy and

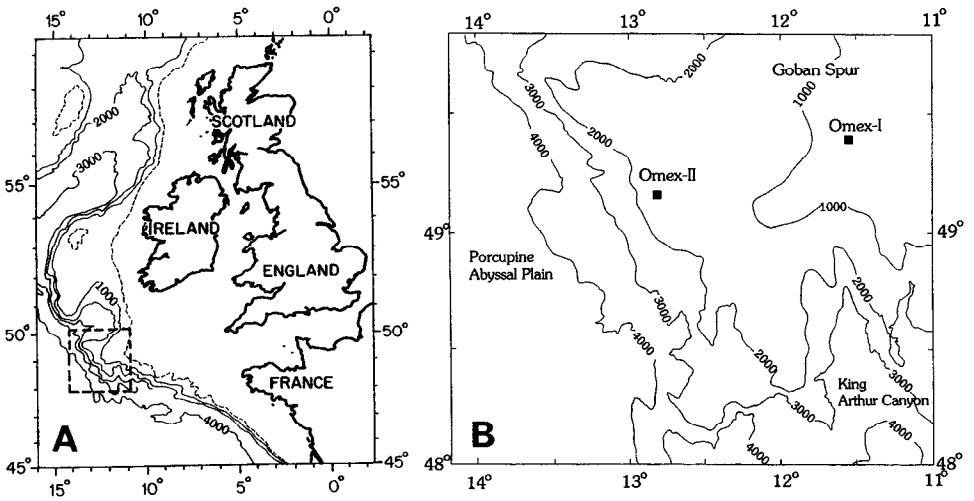

Figure 2. (A) Location of the deep-water continental platform Goban Spur; (B) positions of the stations OMEX-I and OMEX-II.

radiocarbon dating (Van Weering and De Stigter, pers. comm.). More than 90% of the macrofauna at these stations were present in the upper 5 cm of the sediment (Flach and Heip, 1996). This indicates that sediment mixing due to bioturbation was mainly limited to this surface layer. Sediment mixing or biodiffusion coefficients (D_b) calculated from excess ^{210}Pb profiles (Van Weering and De Stigter, pers. comm.), assuming a uniformly mixed surface zone of 5 cm overlying undisturbed sediment, amount to 0.18 and 0.05 $cm^2\ y^{-1}$ at stations I and II, respectively.

3. Experimental methods

a. Sampling. Sediment cores with overlying bottom water were obtained with a cylindrical box corer (either 30 or 50 cm i.d.). Subsamples were taken from the box cores with Plexi-glas or acrylic liners (3.1, 5.4 or 10 cm i.d.) which were closed with rubber stoppers. Only cores without any visible disturbance were used.

b. Pore water analysis. Subcores (3.1 cm i.d.) were sliced into 16 depth intervals down to a depth of 15 cm under nitrogen and at *in-situ* temperature immediately after collection. Pore water was collected from these slices using teflon Reeburgh-type squeezers under N_2-pressure (Reeburgh, 1967) and 0.2 μm cellulose acetate filters. Bottom water samples were obtained from the overlying water in one of the subcores. The samples were immediately analyzed for NH_4^+ (phenol-hypochlorite method; Helder and De Vries, 1979), NO_3^- and HPO_4^{2-} (Strickland and Parsons, 1972). Aliquots of pore water were acidified to pH $\approx$ 1 and analyzed for Fe^{2+} (ferrozine method; Stookey, 1970) and Mn^{2+} (formaldoxime method; Brewer and Spencer, 1971). All analyses were carried out on a Technicon

TRAACS-800 autoanalyzer. The analytical precision of the determinations was 2% for NH_4^+ and HPO_4^{2-} and 1% for all other compounds. The acidified pore water samples were additionally analyzed for HPO_4^{2-} to determine whether loss of pore water HPO_4^{2-} due to Fe^{2+} oxidation and subsequent sorption of HPO_4^{2-} (Bray *et al.*, 1973) had occurred in the sample cups. No significant difference in the pore water HPO_4^{2-} concentration in acidified and nonacidified pore water samples was found.

Pore water O_2 profiles were determined in subcores (5.4 cm i.d.) on-deck with Clark type micro-electrodes (Diamond Corporation, type 737, 60 μm tip diameter; further details will be given in Epping *et al.*, in prep.).

c. Solid phase analysis. The sediment remaining after the collection of the pore water was dried (60°C) and ground (teflon mortar and pestle) to <125 μm. These samples were used for all subsequent solid phase analyses. Inorganic sediment P was fractionated in to Fe-bound P, authigenic P (this includes CFA, biogenic Ca-P, $CaCO_3$-bound P and possibly smectite-bound P) and detrital Ca-P using a sequential extraction procedure modified from the sedex method of Ruttenberg (1992). Fe-bound P was determined as citrate-dithionite bicarbonate (CDB, pH = 7.3, 8 h, 20°C) extractable P. The sediment residue was subsequently extracted with 1 M Na-acetate buffer (pH = 4, 6 h, 20°C) and treated with a 1 M $MgCl_2$ (pH = 8, 0.5 h, 20°C) wash solution. Authigenic P was calculated as the sum of the P extracted in these last two steps. The sediment residue was then treated with 1 M HCl (24 h, 20°C) and the amount of extracted P was used as a measure of detrital Ca-P. There are three differences with the original 13-step procedure of Ruttenberg (1992). First, the 1 M $MgCl_2$ step to extract exchangeable or loosely sorbed P was omitted. Our Fe-bound P fraction thus includes easily exchangeable P. Second, we omitted all but one of the $MgCl_2$ washes and all H_2O rinses. These were included in the original procedure to reverse secondary sorption of P on to residual solid surfaces during the extractions. The results of Ruttenberg (1992) show, however, that this process is not important during the CDB and HCl extractions and can be largely reversed with only one $MgCl_2$ extraction following the acetate buffer treatment. Third, we determined organic P in a separate procedure, since organic P concentrations may be underestimated when using the sequential sedex procedure (Ruttenberg, 1992; Berner *et al.*, 1993).

Organic P was determined nonsequentially as the difference between 1 M HCl extractable P (24 h) before and after ignition of the sediment (550°C, 2 h; Aspila *et al.*, 1976). Total P is calculated as the sum of this organic P and the inorganic P determined with the sequential procedure. Inorganic P concentrations determined as the sum of Fe-bound P, authigenic P and detrital Ca-P were approximately equal to P concentrations obtained with the 1 M HCl extraction in the one-step procedure. Only at some depth intervals in the upper 2 cm at stations I and II significantly more P (up to ~1 μmol g^{-1}) was extracted with the sequential procedure. We attribute this discrepancy to incomplete extraction of inorganic P (most probably of Fe-bound P) with 1 M HCl.

All extractions were performed in duplicate. The P concentration in the CDB extracts

(Fe-bound P) was determined using an Inductively Coupled Plasma-Atomic Emission Spectrophotometer (ICP-AES; Spectro Analytical Instruments). All other P analyses were carried out using a Shimadzu Spectrophotometer with the method of Strickland and Parsons (1972). Precision of the individual extractions was generally ~5%. As the organic P concentration was determined as the relatively small difference between two large numbers, the uncertainty in the organic P concentrations is large (up to 30%).

The Fe and Mn concentrations in the CDB solutions of the P-extractions were measured using an ICP-AES and a Perkin Elmer 5100 PC Atomic Absorption Spectrophotometer, respectively. CDB-extractable Fe is assumed to be a measure of total Fe bound in Fe oxides (CDB may also extract some Fe from clay minerals and from Fe sulfides; Slomp *et al.*, 1996). CDB extractable Mn is used as a measure of the total Mn oxides in the sediment (Canfield *et al.*, 1993).

Total C and N and organic C were measured on a Carlo Erba 1500-2 elemental analyzer. Organic C was determined as the concentration of C in the sample after treatment with sulfurous acid (Verardo *et al.*, 1990). $CaCO_3$ content was calculated from inorganic C concentrations determined as the difference between total and organic C. All sediment N was assumed to be present in an organic form. Grain size distribution was measured with a laser diffraction particle sizer (Malvern 2600 E). Sediment porosity was measured in samples from three additional subcores (3.1 cm i.d.). These were sliced into 10 depth intervals (slices of 0.5 cm thickness down to a depth of 5 cm) and the samples were dried at 105°C (24 h).

4. Description of the model

To obtain more quantitative insight in the redistribution of sediment P with depth, a mathematical model describing the sedimentary P cycle, as outlined in Figure 1, was developed and applied to the data. The steady-state model describes the concentration change with depth of pore water HPO_4^{2-}, and three forms of particulate P, i.e., organic P, Fe-bound P and authigenic P. The latter phase is assumed to include all P phases extractable with acetate buffer (see Section 3c). Transport of solid phase P occurs through bioturbational/physical mixing (described as a biodiffusion process) and sediment accumulation. Transport of dissolved HPO_4^{2-} additionally takes place through molecular diffusion.

The sediment column is divided into three zones: an oxidized surface zone (I: $0 \leq x \leq L_1$), a reduced sediment zone with bioturbation (II: $L_1 < x \leq L_2$) and a reduced sediment zone without bioturbation (III: $x > L_2$). The processes included are (1) release of HPO_4^{2-} from organic P due to organic matter mineralization (zone I, II, III), (2) reversible sorption of HPO_4^{2-} to Fe oxides (zone I), (3) release of HPO_4^{2-} from Fe-bound P due to reductive dissolution of the Fe oxides (zone II, III) and (4) CFA precipitation (zone II, III). All release and removal processes are described as first-order reactions, with the rate being equal to a rate constant times the difference between the actual concentration and an equilibrium (pore water) or asymptotic (solid phase) value. The rate constants for the processes (1) to (4) listed above are k_g, k_s, k_m, and k_a, respectively. The pore water

equilibrium concentrations for sorption and CFA precipitation are C_s and C_a. The asymptotic Fe-bound P and organic P concentrations are equal to M_∞ and G_∞.

There are two major differences with the only other diagenetic P model known to us that includes both HPO_4^{2-} release from organic matter and release from Fe oxides (Van Capellen and Berner, 1988). Firstly, we include transport through bioturbational/physical mixing in the upper part of the sediment. This increases the downward transport of organic and Fe-bound P and thus enhances the cycling of P in the sediment (as shown for the Mn cycle by Aller (1990)). Furthermore, this results in upward transport of CFA and thus in a "background" concentration of CFA at the sediment-water interface. Secondly, sorption of HPO_4^{2-} is modeled as a first-order process and not as simple linear equilibrium sorption. Sorption isotherms for oxic sediments may deviate from linearity, and P sorption has been shown to be rapid but not instantaneous (e.g. Slomp and Van Raaphorst, 1993). Description of P sorption as a first-order process has proved to be successful in the past (Van Raaphorst *et al.*, 1988, 1990; Van Raaphorst and Kloosterhuis, 1994).

Pore water HPO_4^{2-} and the particulate P forms have units of μmol per cm^3 pore water and μmol per gram of dry sediment, respectively. A conversion factor ϑ (gram of dry sediment per cm^3 of pore water) is introduced to enable a combination of dissolved HPO_4^{2-} and solid phase P in one model:

$$\vartheta = \rho_s[(1 - \phi)/\phi] \tag{1}$$

where ρ_s is the average density of the sediment particles (2.65 g cm^{-3}) and ϕ is the porosity of the sediment (in units of $cm^3\ cm^{-3}$). The molecular (D_s) and biodiffusion (D_b) coefficients (both in units of $cm^2\ d^{-1}$), the sedimentation rate (ω, in units of cm d^{-1}), the reaction rate constants (k_g, k_s, k_m and k_a, in units of d^{-1}) and the sediment porosity (ϕ) are assumed to be constant with depth in each relevant layer. This is a common assumption in many diagenetic models (e.g. Berner, 1980).

The set of differential equations for the one-dimensional distribution of pore water HPO_4^{2-} and the three particulate P forms is given in the Appendix (A1–A12). These equations were solved analytically assuming continuity in concentrations and fluxes of both dissolved HPO_4^{2-} and solid phase P at the boundaries between the three depth zones, i.e. at $x = L_1$ and $x = L_2$, and considering appropriate boundary conditions for the system at $x = 0$ and $x \rightarrow \infty$. Constant fluxes of organic P, Fe-bound P and authigenic P from the overlying water to the sediment were assumed at $x = 0$ ($J_{G_{x=0}}$, $J_{M_{x=0}}$ and $J_{A_{x=0}}$, respectively). The pore water HPO_4^{2-} concentration at $x = 0$ was assumed to be equal to the bottom water concentration (C_o). When $x \rightarrow >\infty$, equilibrium values for pore water HPO_4^{2-} (C_a), and asymptotic values for organic and Fe-bound P (G_∞, M_∞) are assumed to be reached. The mathematical expressions for these boundary conditions are given in the Appendix (A13–A35).

It is important to note that three processes can contribute to a 'background' concentration of authigenic P at the sediment-water interface: (1) formation of CFA in the surface layer of the sediment, (2) upward bioturbational/physical transport of CFA formed *in-situ*

Table 1. Sediment characteristics of the surface layer (0–0.25 cm) at stations OMEX-I and -II. The sediment classification is based on the Wentworth size scale (Pettijohn *et al.*, 1972).

	Unit	OMEX-I	OMEX-II
porosity	(v/v)	0.50	0.48
org. C	(wt%)	0.37	0.64
org. N	(wt%)	0.05	0.09
$CaCO_3$	(wt%)	51	61
median grain size	(μm)	92	55
sed. fraction <2 μm	(%)	0	5
sed. classification		very fine sand	coarse silt

in deeper layers and (3) deposition of authigenic P which has been formed elsewhere ($J_{A_{x=0}}$). In the model, it is assumed that the first process is not important when an oxidized surface layer is present. This is a reasonable assumption when sorption of HPO_4^{2-} to Fe-oxides in the oxidized layer is rapid. This results in a buffering of pore water HPO_4^{2-} concentrations to low values in the surface sediment thus presumably precluding supersaturation of the pore water with respect to CFA. The contribution of the other two processes to the background concentration of authigenic P can be calculated with the model when L_1, L_2, D_s, D_b and ω are fixed.

Values of k_g, k_s, k_m, k_a, $J_{G_{x=0}}$, $J_{A_{x=0}}$, G_∞, and M_∞ were varied to fit the model to experimental data. Variance-weighted sums of squares of all four components were minimized simultaneously using an iteratively reweighted regression (Draper and Smith, 1967). This means that 8 fit parameters were used for 4 profiles with a total of 64 data points. The other parameters (L_1, L_2, D_s, D_b, ω, C_o, C_s, C_a, $J_{M_{x=0}}$) were fixed based on existing data.

5. Experimental results

a. General sediment characteristics. Some general sediment characteristics of the two stations are listed in Table 1. Both sediments have a low porosity, are organic-poor and contain substantial amounts of $CaCO_3$, mainly in the form of foraminiferal remains. The sediment from station II is finer grained and contains higher concentrations of organic C and N and $CaCO_3$ than that from station I.

At both stations, $CaCO_3$ concentrations decrease with depth (Fig. 3A and B). This decrease is confined to the surface 6 cm of the sediment at station I, whereas it occurs between 6 and 14 cm depth at station II. The organic C profile at station I displays a large degree of scatter (Fig. 3C). At station II, organic C concentrations decrease sharply close to the sediment-water interface followed by a more gradual decrease with depth (Fig. 3D). Organic N concentrations rapidly decrease in the upper 2 cm of the sediment at station I, succeeded by relatively constant values with depth (Fig. 3E). At station II, the organic N profile closely follows the trend of the organic C profile (Fig. 3F). Sediment porosity decreases slightly with depth at both stations. The sediment grain size distribution does not

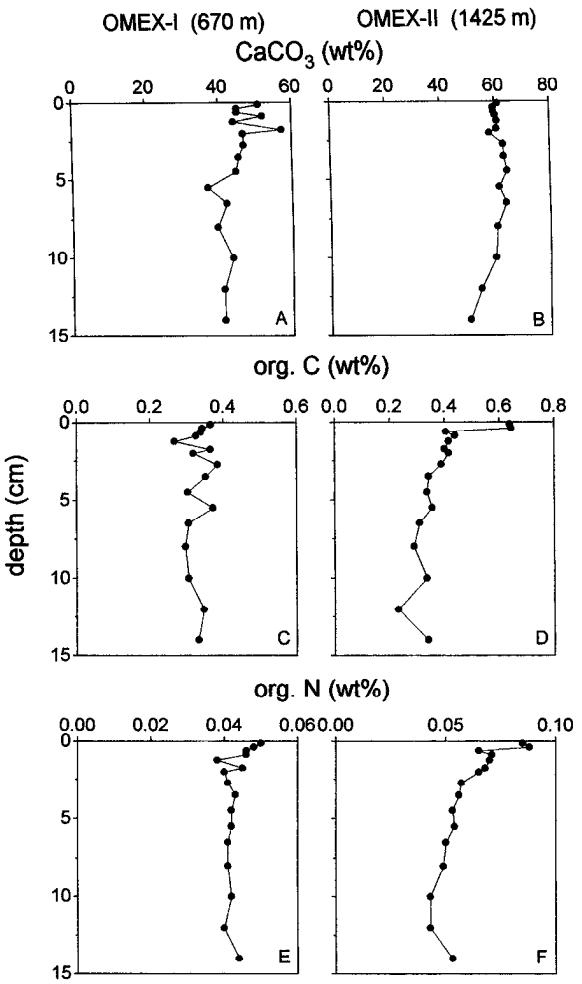

Figure 3. Profiles of (A, B) $CaCO_3$, (C, D) organic C and (E, F) organic N (wt%) at stations OMEX-I and -II.

change significantly with depth at station I, but the amount of fine sediment material increases between 10 and 15 cm depth at station II (the median grain size decreases from 50 μm to 23 μm in this depth interval).

b. Pore water profiles. Bottom water O_2 concentration levels were 231 and 241 μmol dm^{-3} at stations I and II, respectively, and were close to saturation values. Maximum O_2 penetration depths were shallower at station I (0.91 cm) than at station II (5.0 cm; complete profiles will be given in Epping *et al.*, in prep.). Pore water NO_3^- concentrations (Fig. 4A and B) reached a maximum close to the sediment surface at both stations. At station I, NO_3^- concentrations rapidly decreased to low values within the upper 2 cm of the

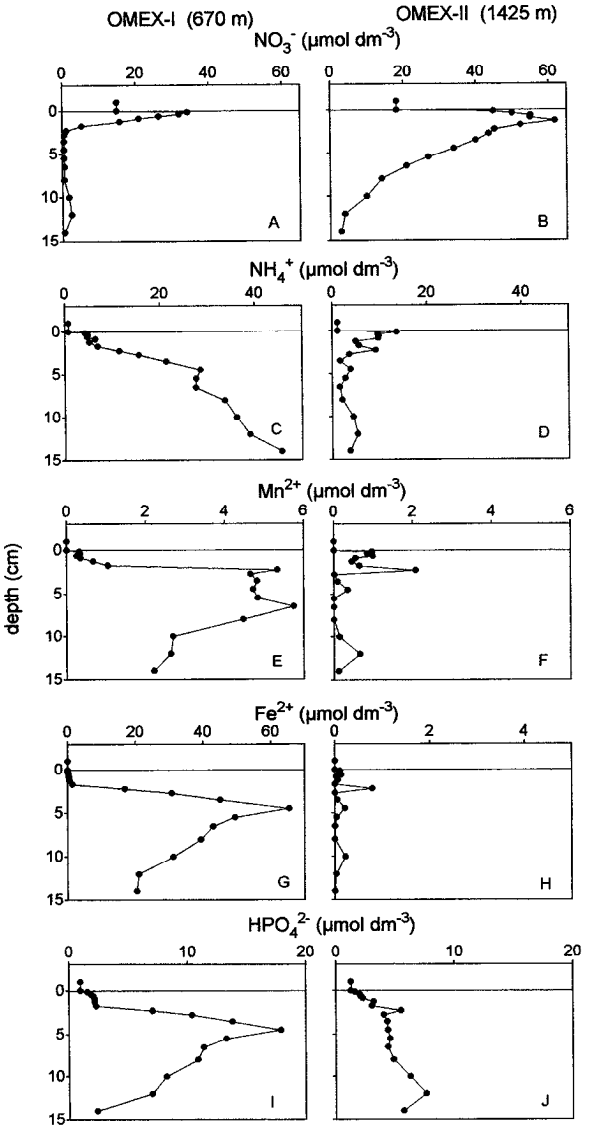

Figure 4. Pore water profiles of (A, B) NO_3^-, (C, D) NH_4+, (E, F) Mn^{2+}, (G, H) Fe^{2+} and (I, J) HPO_4^{2-} (µmol dm^{-3}) at stations OMEX-I and -II.

sediment, whereas at station II, NO_3^- penetrated down to 14 cm depth. In the following text, we will use (1) the maximum depth of O_2 penetration as the boundary between the *oxic* and *anoxic* sediment zones and (2) the depth where NO_3^- concentrations reach a background value as the boundary between the *oxidized* and *reduced* sediment zones, as relevant for Fe.

Pore water NH_4^+ concentrations rapidly increased with depth (to ~45 μmol dm^{-3} at 15 cm) in the reduced zone at station I (Fig. 4C). At station II, the NH_4^+ profile reached a maximum (~14 μmol dm^{-3}) close to the sediment-water interface, followed by a decrease to concentrations below ~5 μmol dm^{-3} at depth (Fig. 4D). Mn^{2+} and Fe^{2+} pore water profiles indicate dissolution of sediment Mn and Fe oxides upon NO_3^- depletion at station I (Fig. 4E and G). At station II, pore water Mn^{2+} and Fe^{2+} concentrations were very low (<2 μmol dm^{-3}) throughout the sediment (Fig. 4F and H).

The pore water HPO_4^{2-} profile at station I shows a remarkable resemblance to the Fe^{2+} profile, suggesting a coupling between the release of HPO_4^{2-} and Fe^{2+} in the sediment (Fig. 4G and I). HPO_4^{2-} concentrations are buffered to low values (~1–2 μmol dm^{-3}) in the oxidized surface zone of the sediment. The sharp increase in the HPO_4^{2-} concentration with depth below this zone (to ~18 μmol dm^{-3}) is followed by a steep decrease below ~5 cm, indicating removal of dissolved HPO_4^{2-} in the reduced part of the sediment. At station II, the HPO_4^{2-} profile has a distinctly different shape (Fig. 4J). The HPO_4^{2-} concentration increases immediately below the sediment-water interface but the gradient levels off below 2.5 cm. The maximum HPO_4^{2-} concentration reached (~8 μmol dm^{-3}) is much lower than at station I. The small but simultaneous maxima of Mn^{2+}, NH_4^+, Fe^{2+} and HPO_4^{2-} in the 2–2.5 cm depth interval, suggest very local, reduced conditions due to organic matter decomposition in the oxidized sediment at station II (Fig. 4D, F, H and J).

c. Solid phase profiles of Mn, Fe and P. The sharp subsurface peak in sediment Mn oxide (Fig. 5A) at station I is typical for mobilization and reprecipitation of Mn at the redox interface for Mn in a low sedimentation and low bioturbation sediment environment (Burdige and Gieskes, 1983). The redox interface for Mn is generally assumed to occur at the oxic/anoxic interface (Aller, 1990). The depth of the solid phase Mn and pore water Mn^{2+} peaks at station I indicate that either the on-deck O_2 profiles underestimate actual *in-situ* O_2 penetration or that NO_3^- is acting as the main oxidant for Mn^{2+}. At station II, Mn oxide concentrations decrease with depth but show a large variability (Fig. 5B). Several of the local minima in the Mn oxide profile occur in the same depth intervals as maxima in the pore water Mn^{2+} profile (2–2.5, 4–5 and 11–13 cm; Fig. 4F). This suggests that the observed variability in the Mn oxide profile is due to local Mn oxidation and reduction in the 'oxidized' sediment of station II.

A decrease in total Fe oxides with depth is observed at both stations (Fig. 5C and D) with the largest decrease occurring in the upper 2 cm of the sediment. This is followed by a more gradual decrease down to ~8 and ~6 cm at stations I and II, respectively. Reduction of Fe oxides apparently occurs in the 'oxidized' sediment zone at station II.

The sediment P profiles, as determined with the selective extractions, are shown in Figure 6A–H. Organic P (Fig. 6A and B) remains relatively constant or even slightly increases with depth at station I, whereas a decrease is observed at station II. At both stations, a decrease of Fe-bound P and a concomitant increase of authigenic P (Fig. 6C and

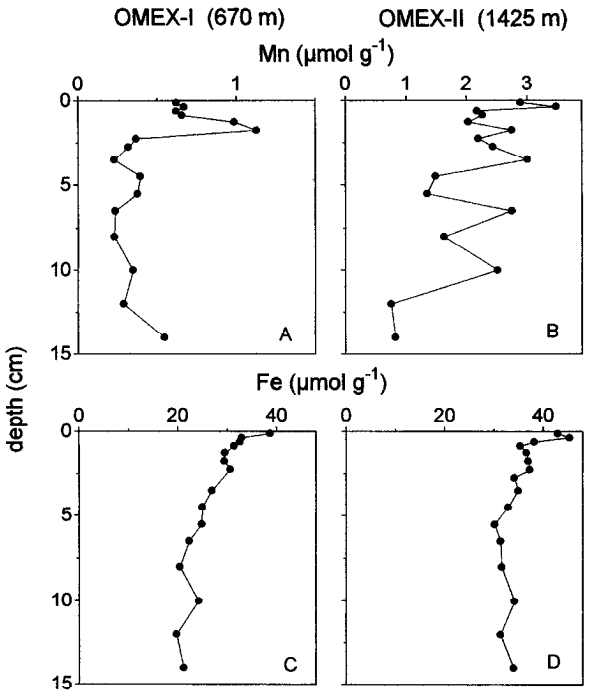

Figure 5. Solid phase profiles of CDB-extractable (A, B) Mn and (C, D) Fe (μmol g^{-1}) at stations OMEX-I and -II.

D) with depth was found. Detrital Ca-P concentrations (Fig. 6E and F) are relatively constant at station I, but slightly increase with depth at station II. At station I, inorganic and total P concentrations (Fig. 6G and H) increase slightly with depth. At station II, inorganic P concentrations remain relatively constant with depth, whereas total P concentrations decrease.

The acetate extraction is not strictly selective for CFA (see Section 3c and Ruttenberg, 1992). If foraminiferal shells contain little P, as suggested by the results of Sherwood *et al.* (1987), an increase of the contribution of $CaCO_3$ to the total sediment flux with time may result in a dilution of acetate extractable P phases which have not been formed *in-situ.* Consequently, lower concentrations of authigenic P will be found at the sediment-water interface than at depth without in-situ CFA formation. In this study, $CaCO_3$ concentrations decreased with depth at both stations (Fig. 3A and B). This can be the result of an increase in the contribution of $CaCO_3$ to the sediment flux with time. To assess whether this could account for the observed authigenic P increase, authigenic P concentrations are presented on a $CaCO_3$-free basis in Figure 6 I and J. The results suggest that admixing with $CaCO_3$ cannot account for the increase of authigenic P observed at station I, but may be responsible for a large part of the observed increase with depth at station II.

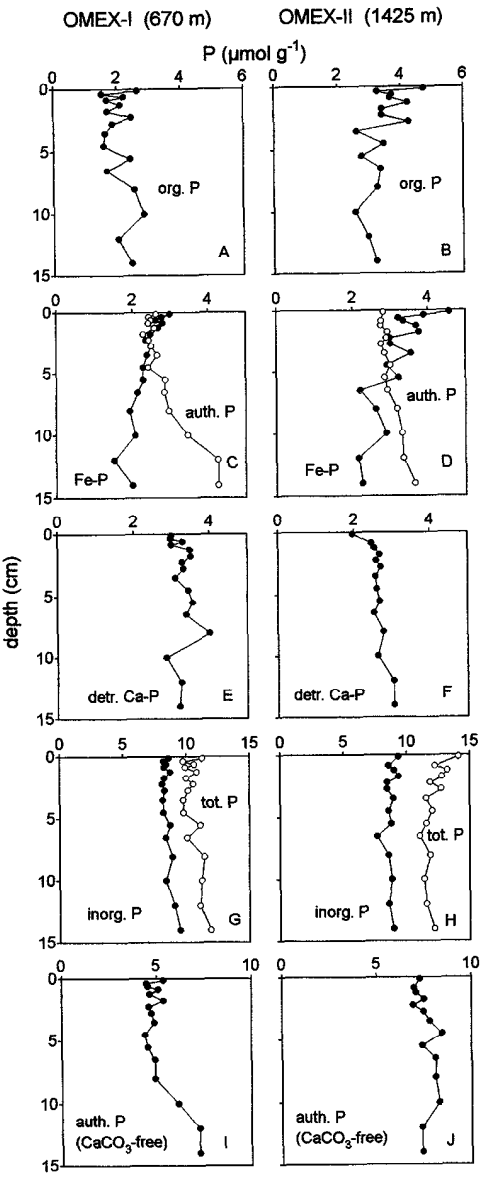

Figure 6. Solid phase profiles of P (μmol g^{-1}) at stations OMEX-I and -II as determined with the extraction procedures: (A, B) organic P, (C, D) Fe-bound P (filled circles) and authigenic P (open circles), (E, F) detrital Ca-P, (G, H) inorganic P (filled circles) and total P (open circles) and (I, J) authigenic P on a $CaCO_3$ free-basis.

Table 2. Values of the fixed parameters as used in the diagenetic P model.

Parameter	Description	Units	Value	Source
L_1	boundary oxidized/reduced zone	cm	2.0	depth where NO_3^- reaches background values (Fig. 4)
L_2	boundary bioturbated/non-biot. zone	cm	5.0	macrofaunal densities (see study sites)
ϕ	sediment porosity	$cm^3\ cm^{-3}$	0.43	mean porosity top 5 cm
D_s	whole sediment diffusion coeff.	$cm^2\ d^{-1}$	2.1×10^{-1}	Krom and Berner (1980)
D_b	sed. mixing or biodiffusion coeff.	$cm^2\ d^{-1}$	4.9×10^{-4}	Van Weering & De Stigter (pers. comm.)
ω	sedimentation rate	$cm\ d^{-1}$	6.9×10^{-6}	Van Weering & De Stigter (pers. comm.)
C_o	overlying water HPO_4^{2-} conc.	$\mu mol\ cm^{-3}$	9.1×10^{-4}	measured between water concentration
C_s	equilibrium conc. for P sorption	$\mu mol\ cm^{-3}$	1.0×10^{-3}	Froelich (1988), Slomp & Van Raaphorst (1993)
C_a	equilibrium conc. for CFA prec.	$\mu mol\ cm^{-3}$	3.7×10^{-3}	Atlas & Pytkowicz (1977), assuming pH = 7.5
$J_{M_{x=0}}$	flux of Fe-bound P to the sediment	$\mu mol\ cm^{-2}\ d^{-1}$	0.2×10^{-4}	see text

6. Application of the model

Both the pore water and solid phase profiles indicate that reduction of Fe and Mn oxides occurs in the oxidized sediment of station II, thus implying a strong heterogeneity of the sediment at this station. As the model is based on a strictly vertical redox zonation, it cannot be applied to the results of station II and we will therefore concentrate on station I.

a. Fixed parameters. The fixed parameters used for the model fits and their source are listed in Table 2. The burial flux of Fe is calculated from the sediment accumulation rate (Table 2) and the Fe concentration of the material being buried (Fig. 5). Assumption of steady-state requires that all Fe thus removed through burial is replenished through sedimentation of Fe oxides. As these Fe oxides necessarily contain some P, this results in a flux of Fe-bound P to the sediment ($J_{M_{x=0}}$). The Fe/P ratio of the sedimenting material is of course crucial for the value of this P flux. We assume the Fe/P ratio of these incoming Fe oxides to be equal to 10, which is a value typical for both synthetic (Gerke and Hermann, 1992) and natural (Jensen and Thamdrup, 1993; Sundby *et al.,* 1992; Slomp *et al.,* 1996) poorly crystalline Fe oxides.

b. Model fits and calculated rate constants. Model fits for pore water HPO_4^{2-} and the three diagenetically active solid phase P forms agree reasonably well with the measured profiles

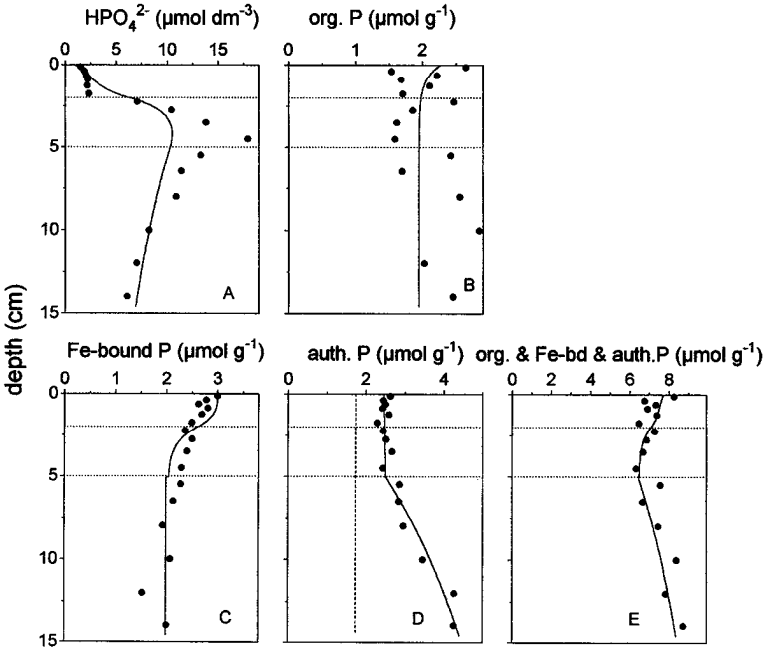

Figure 7. Model fits (solid lines) to profiles of (A) pore water HPO_4^{2-} (µmol dm^{-3}), (B) organic P, (C) Fe-bound P and (D) authigenic P (all three in µmol g^{-1}) for station OMEX-I. The dotted lines in each panel indicate the boundaries between the oxidized and reduced sediment zones (L_1 = 2 cm) and between the bioturbated and nonbioturbated zones (L_2 = 5 cm). The dashed line in panel (D) is the profile of the authigenic P which has not been formed *in situ*. The profile in panel (E) is the sum of the solid phase P forms (B, C, D) and the solid line is the sum of their model fits.

(Fig. 7A–D). The major discrepancy between the model and field results occurs for the pore water HPO_4^{2-} profile (Fig. 7A). The sharp transition from low concentrations in the oxidized sediment zone to 'peak values' below the redox boundary is not accurately described. Due to the large scatter in the organic P data (Fig. 7B), it is difficult to check the validity of the model fit for this component. The organic C profile is of little assistance, as a large variability was also observed in this profile (Fig. 3C). The sharp decrease in organic N (Fig. 3E) in the upper 2 cm of the sediment, however, supports the modeled decrease of organic P with depth. The results of the model calculations indicate that CFA formation can account for the increase of authigenic P with depth at station I. Fitted values for $J_{G_{x=0}}$, $J_{A_{x=0}}$, G_∞ and M_∞ and for the rate constants k_s, k_g, k_m and k_a are listed in Table 3.

7. Discussion

a. Diagenetic redistribution of P. Pore water profiles of NO_3^-, Mn^{2+} and Fe^{2+} indicate the presence of an oxidized surface zone of ~2 cm overlying reduced sediment at station I. Both the solid phase P (Fig. 6) and pore water HPO_4^{2-} and Fe^{2+} (Fig. 4) profiles at this

Table 3. Values of the fitted parameters for station OMEX-I.

Parameter	Description	Units	Value
$J_{G_{x=0}}$	flux of organic P to the sediment at $x = 0$	μmol cm^{-2} d^{-1}	3.11×10^{-4}
$J_{A_{x=0}}$	flux of authigenic P to the sediment at $x = 0$	μmol cm^{-2} d^{-1}	0.18×10^{-4}
G_∞	asymptotic conc. for organic P	μmol g^{-1}	1.94
M_∞	asymptotic conc. for Fe-bound P	μmol g^{-1}	1.99
k_s	rate constant for P sorption	d^{-1}	2.6×10^{-1}
k_g	rate constant for organic P decomposition	d^{-1}	7.4×10^{-4}
k_m	rate constant for Fe-bound P release	d^{-1}	5.3×10^{-4}
k_a	rate constant for CFA precipitation	d^{-1}	1.0×10^{-3}
k'_g	$k_g \times \vartheta$	d^{-1}	2.5×10^{-3}
k'_m	$k_m \times \vartheta$	d^{-1}	1.8×10^{-3}

station suggest a redistribution of Fe-bound P to an authigenic P phase in the reduced part of the sediment. The model results (Fig. 7) support this view and show that CFA formation can account for the increase of authigenic P at station I. The discrepancy between the pore water model and field results close to the redox-boundary may be explained by the fact that pore water profiles are much more sensitive indicators of short-term, non-steady state events than solid phase profiles. This is illustrated in Figure 8, which shows the results of a scenario in which the model was fit to the pore water HPO_4^{2-} profile and the corresponding Fe-bound P and authigenic P profiles were subsequently calculated. The organic P profile was assumed to be similar to that of Fig. 7 and deposition of authigenic P from the overlying water was assumed to be absent ($J_{A_{x=0}} = 0$). The sharp peak in the pore water HPO_4^{2-} profile clearly does not match with the measured Fe-bound P and authigenic P profiles. These results can be explained by a very temporary increase of the sediment mixing rate, resulting in a temporary increase of the release of HPO_4^{2-} from Fe oxides in the reduced sediment zone. It is also important to note that uniform rate constants, transport coefficients and equilibrium concentrations throughout each sediment zone are assumed in the model, whereas in reality these will vary with depth, particularly close to the redox boundary. Thus the model gives an overly simplistic description of the complex HPO_4^{2-} sorption, precipitation and release processes.

To illustrate the extent to which the pore water HPO_4^{2-} profile is modified by authigenic P formation, the model results of Figure 7 are compared to a model scenario in which CFA precipitation is absent and the profiles of Fe-bound P and organic P remain unchanged (Fig. 9). The results show that CFA precipitation suppresses pore water HPO_4^{2-} concentrations and is responsible for the downward gradient of the profile below ~4 cm depth. That Fe-bound P and not organic P is acting as the main source of pore water HPO_4^{2-} at station I, is illustrated in Figure 10. Here, the model fits of Figure 7 are compared to a model scenario in which Fe-bound P plays no role. The results show that a much larger decrease of organic P with depth than could ever be supported by the measured profile must be invoked to explain the profiles of HPO_4^{2-} and authigenic P.

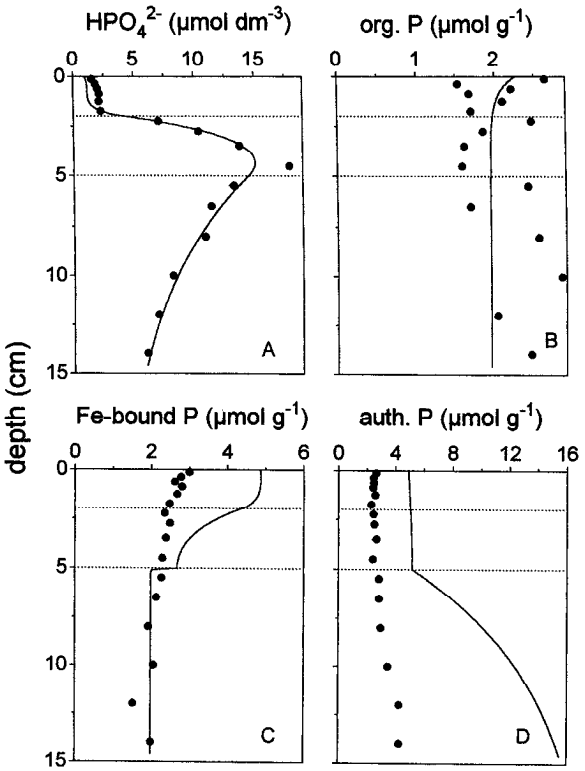

Figure 8. The model fit (solid line) to the profile of (A) pore water HPO_4^{2-} (µmol dm^{-3}) and model calculated (solid lines) profiles of (B) organic P, (C) Fe-bound P and (D) authigenic P (all three in µmol g^{-1}) for station OMEX-I. The dotted lines in each panel indicate the boundaries between the oxidized and reduced sediment zones (L_1 = 2 cm) and between the bioturbated and nonbioturbated zones (L_2 = 5 cm). k_s = 2.3 d^{-1}, k_a = 4.7 × 10^{-3} d^{-1}, k_m = 2.0 × 10^{-4} d^{-1} and $J_{A_{x=0}}$ = 0 µmol cm^{-2} d^{-1}. All other parameters are as in Tables 2 and 3.

Comparison of the rate constants obtained for the model fits of Figure 7 (Table 3) to rate constants observed in other sediments should provide insight into the validity of the model calculations. Very little is known, however, about the actual *in-situ* rate constants for the reactions controlling pore water HPO_4^{2-} concentrations in marine sediments. Estimates from diagenetic models for P are only available for the rate constants for sorption (k_s) and authigenic apatite formation (k_a). The present value of the sorption rate constant k_s falls within the lower part of the range of 0.1–23.8 d^{-1} estimated for sandy North Sea sediments (Van Raaphorst *et al.*, 1990). Van Cappellen and Berner (1988) estimated a first-order rate constant of 0.17 d^{-1} for nonsteady state CFA precipitation in a well-defined layer of a Mexican continental margin sediment. The rate constant determined for dispersed, steady state CFA precipitation (k_a) in our study is substantially lower. Tromp *et al.* (1995) proposed the following relationship between the oxic degradation rate constant for organic

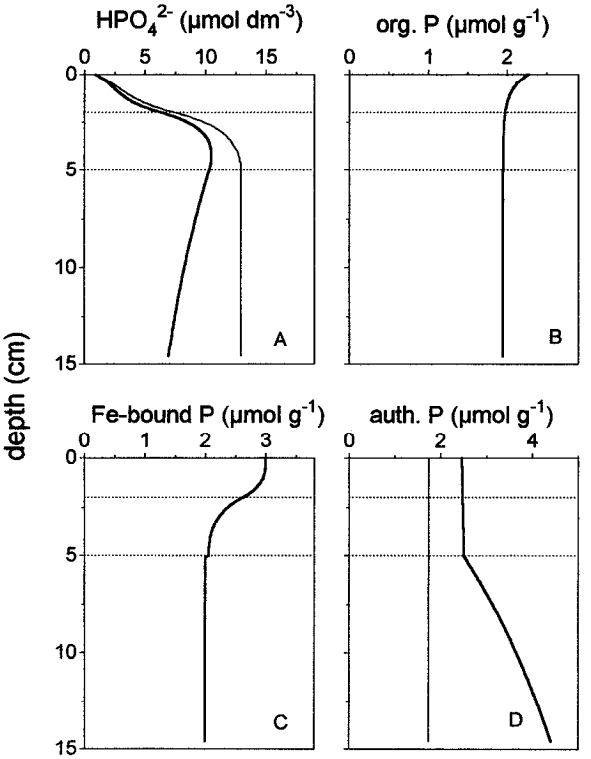

Figure 9. Model results from Figure 7 (thick solid lines) for profiles of (A) pore water HPO_4^{2-} (µmol dm^{-3}), (B) organic P, (C) Fe-bound P and (D) authigenic P (all three in µmol g^{-1}) and results of an alternative model scenario (thin solid lines). The dotted lines in each panel indicate the boundaries between the oxidized and reduced sediment zones (L_1 = 2 cm) and between the bioturbated and nonbioturbated zones (L_2 = 5 cm). For the alternative scenario: $k_a = 1.0 \times 10^{-16}$ d^{-1}, $k_s = 0.2$ d^{-1}. All other parameters are as in Tables 2 and 3.

C (k_c in units of y^{-1}) and sedimentation rate (ω in units of cm y^{-1}):

$$k_c = 2.97\omega^{0.62} \tag{2}$$

With a sedimentation rate of 2.5×10^{-3} cm y^{-1} (Table 2) this gives a k_c of $\sim 2.0 \times 10^{-4}$ d^{-1} for station I. This value is very close to the rate constant for organic P decomposition (k_g) estimated for station I, particularly when taking into account that preferential regeneration of P relative to C oxidation is believed to occur upon oxic decomposition of organic material (Ingall and Van Cappellen, 1990). The rate constant for P release due to reduction of Fe oxides (k_m) observed for station I is lower than most first-order rate constants for reductive dissolution of Fe oxides due to chemical reductants or by microorganisms under laboratory conditions (Lovley, 1991; Schwertmann, 1991; Stumm and Sulzberger, 1992). Canfield *et al.* (1992), for example, calculated values ranging from 6.0 d^{-1} for amorphous Fe oxide to 0.03 d^{-1} for synthetic hematite upon

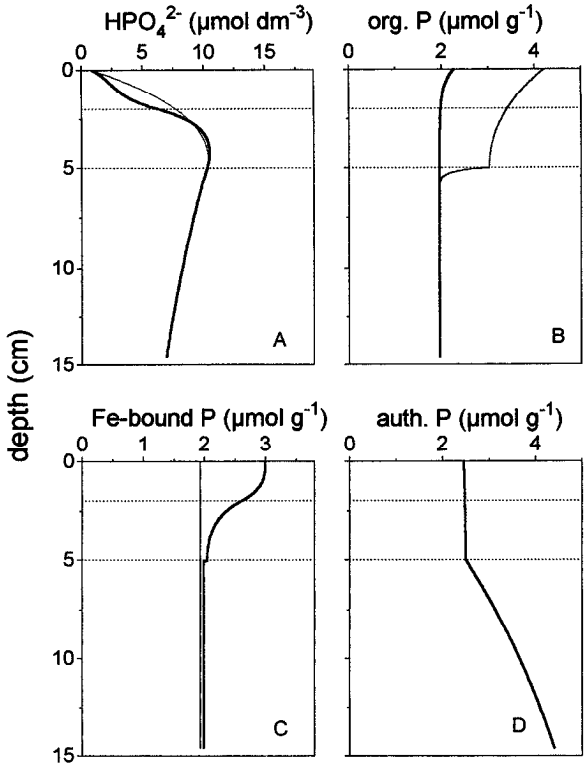

Figure 10. As in Figure 9. For the alternative scenario: $k_s = 1.0 \times 10^{-16}$ d^{-1}, $k_m = 1.0 \times 10^{-16}$ d^{-1}, $k_g = 3.8 \times 10^{-5}$ d^{-1} and $J_{G_{x=0}} = 4.5 \times 10^{-4}$ µmol cm^{-2} d^{-1}.

reduction of these Fe oxides with sulfide (1 mM). We conclude that, with the exception of k_g, the values of the rate constants calculated here are lower than most values obtained in other modeling or laboratory studies, thus suggesting less optimal conditions for the relevant processes in the sediment at station I.

At station II, pore water Fe^{2+}, Mn^{2+}, HPO_4^{2-}, NH_4^+ (Fig. 4) and solid phase Mn (Fig. 5) profiles suggest the occurrence of locally reduced spots associated with organic matter decomposition at several depths in an otherwise oxidized sediment. This concept of micro-environments has been suggested previously to explain both Mn reduction (Kalhorn and Emerson, 1984; Heggie *et al.*, 1986) and SO_4^{2-} reduction (Jørgensen, 1977) in the 'oxic' zone of several sediments. Apparently, organic matter degradation is so rapid locally that the consumption of O_2 is faster than the resupply by molecular diffusion. As O_2 is supplied from the overlying water, most of the Fe^{2+} and Mn^{2+} diffusing out of such micro-sites will be oxidized at the 'top' of each site. When these micro-sites are quantitatively important in a sediment and the rate of sediment accumulation is low, this can eventually result in the net decrease in the amount of Mn and Fe oxides with depth observed here. The results of the sediment P extractions (Fig. 6) suggest that a redistribu-

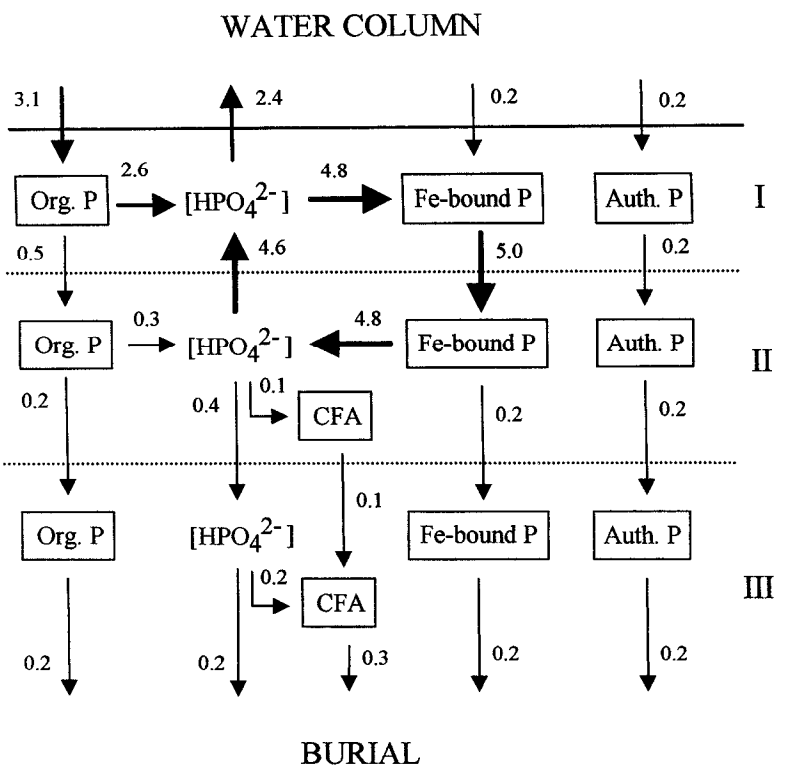

Figure 11. Fluxes of P (in 10^{-4} μmol cm^{-2} d^{-1}) between the pore water and the sediment P reservoirs as calculated with the model for each sediment zone at station OMEX-I. Zone I ($0 \leq x \leq 2$ cm) is the oxidized surface zone. Zone II (2 cm $< x \leq 5$ cm) is the reduced sediment zone with bioturbation. Zone III ($x > 5$ cm) is the reduced sediment zone without bioturbation.

tion of Fe-bound P to CFA may be occurring in these micro-sites below ~6 cm depth at station II. We cannot exclude, however, the possibility that the increase of authigenic P with depth at this station is not due to *in-situ* formation of authigenic P but is the result of a gradual change in the flux of $CaCO_3$ to the sediment with time.

In conclusion, the results indicate that CFA may be forming at the expense of Fe-bound P in both Goban Spur sediments. We will concentrate on the results of station I in the further discussion, as the results for this station are less equivocal than those for station II.

b. A key role for Fe-bound P in CFA formation. Further insight into the mechanism responsible for the early diagenetic redistribution of Fe-bound P to CFA at station I is provided by the fluxes of P between the sediment P reservoirs and pore water HPO_4^{2-} in each sediment zone. These fluxes were calculated with the model and are presented in Figure 11. Combining Figure 7 and 11, the following description of the sedimentary P cycle results.

Most P deposited at the sediment-water interface is associated with organic matter. A large proportion (~85%) of this organic P is decomposed in the oxidized surface layer. Most of the thus-produced pore water HPO_4^{2-} is released very close to the sediment-water interface and immediately escapes to the overlying water. Some of this HPO_4^{2-} is sorbed to Fe oxides, however, and enters the intense cycle of P at the redox boundary. This cycle of P, which is mainly driven by bioturbation through downward transport of Fe-bound P, is responsible for the continuously high concentrations of pore water HPO_4^{2-} immediately below the redox boundary. These high HPO_4^{2-} concentrations favour CFA precipitation. Losses from the internal P cycle occurring due to CFA formation and due to diffusive escape of HPO_4^{2-} are compensated for by input of HPO_4^{2-} released from organic matter in the oxidized surface zone. Bioturbation causes the CFA, formed in the reduced, bioturbated zone (between L_1 and L_2), to be mixed upwards into the oxidized zone, accounting for a 'background' concentration of CFA at the sediment-water-interface. The total background concentration of authigenic P is higher, however, due to a flux ($J_{A_{x=0}}$) of authigenic P formed elsewhere. This authigenic P is only truly authigenic, in the sense that its formation has resulted in the removal of reactive P (i.e. potentially biologically available P) from seawater (see Ruttenberg and Berner, 1993), when it has been formed in a marine environment. In the non-bioturbated zone, release of HPO_4^{2-} from organic P and Fe-bound P is small and downward diffusion of HPO_4^{2-} supplies most P for CFA formation. In this zone of the sediment, the CFA profile is no longer disturbed by mixing and the CFA concentration (Fig. 7D) and the sum of organic, Fe-bound and authigenic P (Fig. 7E) gradually increase with depth. This increase will cease when the porewater reaches equilibrium with respect to CFA.

Assuming that all sediment P phases in Figure 11 consist of reactive P, the total downward flux of reactive P at the lower boundary of the sediment interval under study here (at 15 cm depth) becomes 1.1 μmol m^{-2} d^{-1}. CFA formed *in-situ* accounts for ~25% (0.3 μmol m^{-2} d^{-1}) of this downward flux of reactive P. If the pore water HPO_4^{2-} diffusing downward (0.2 μmol m^{-2} d^{-1}) is also incorporated in CFA, this authigenic mineral phase accounts for ~45% of the downward reactive P flux. If Fe-bound P and authigenic P supplied from the overlying water consist of non-reactive P phases, total reactive P burial decreases to 0.7 umol m^{-2} d^{-1}. Now the contribution of CFA formed in-situ to reactive P burial will be ~40% when downward diffusing HPO_4^{2-} is not incorporated in CFA and ~70% when it is.

In the model calculations we assumed a small flux of Fe oxides from the overlying water with an Fe/P ratio of 10. The Fe/P ratio of the Fe oxides being buried was also ~10 at station I (depth interval 13–15 cm, Fig. 5C and Fig. 6D). Since, under steady-state conditions, the flux of Fe-oxides from the overlying water is equal to the burial flux of Fe, the same also holds for the deposition and burial fluxes of Fe-bound P (Fig. 11). The flux of Fe-bound P from the overlying water is only of minor importance for the internal P cycle at the redox interface as this cycle largely depends on in-situ formation of Fe-bound P.

Intercomparison of the rate constants obtained in this study provides more insight in the

kinetics of the relevant processes. To enable the values of k_m and k_g (first-order in the solid phase concentrations of Fe-bound P and organic P) to be compared to those of k_a and k_s (first-order in the pore water HPO_4^{2-} concentration), the former constants were multiplied by ϑ, giving k'_m and k'_g (Table 3). The high k_s value relative to k'_m and k'_g indicates that, as expected, sorption of HPO_4^{2-} to Fe oxides in the oxidized sediment zone is a more rapid process than HPO_4^{2-} release from either organic matter or from Fe oxides. The rate constant for CFA precipitation (k_a) is of the same order of magnitude as k'_m and k'_g. This suggests that both Fe-bound P and organic P are kinetically suited as sources of HPO_4^{2-} for CFA. We conclude that CFA formation is sufficiently rapid to keep up with release of HPO_4^{2-} from both sources. Which of the two actually acts as the source of P for CFA depends on the location in the sediment where the HPO_4^{2-} release occurs and on the availability of sufficient pore water fluoride.

Summarizing, these results illustrate how an intense cycling of P between Fe-bound P and pore water HPO_4^{2-} can account for elevated concentrations of HPO_4^{2-} below the redox boundary, thus promoting early diagenetic CFA formation. This internal P cycle is driven by downward transport of *in-situ* formed Fe-bound P and refueled by P release from organic matter. This mechanism, in which Fe-bound P plays a key role in early diagenetic CFA formation, acting as an intermediate between organic P and CFA, may be of particular importance in marine sediments with low sedimentation rates where organic matter decomposition takes place close to the sediment-water interface. Remineralized HPO_4^{2-} which would otherwise escape to the overlying water is thus largely retained in the sediment. This could also explain why Fe-bound P acts as the P source for CFA in a low sedimentation environment in the Labrador Sea (Lucotte *et al.*, 1994). In terrigenous, high sedimentation continental margin environments where relatively labile organic matter is buried rapidly, there is less need for an intermediate role of Fe-bound P. Here, organic P may act as a direct source of HPO_4^{2-} for CFA as suggested by Ruttenberg and Berner (1993) for Long Island Sound and Mississippi Delta sediments.

c. CFA as a sink for P. The major importance of CFA formation in marine sediments lies in the fact that CFA acts as a permanent sink for reactive P. The contribution of CFA to the total burial flux of reactive P at station I was estimated to range between ~25 and 70%, depending on whether downward diffusing HPO_4^{2-} is assumed to be incorporated in CFA and whether Fe-bound and authigenic P supplied from the overlying water are assumed to consist of reactive P. This indicates that CFA is a very important sink for reactive P in this sediment. Ruttenberg (1993) estimated a contribution of authigenic P to global reactive P burial of ~28 to 50% based on P speciation results for only three locations: the two high sedimentation, continental margin sites from the study of Ruttenberg and Berner (1993) and one pelagic sediment in the equatorial Atlantic. Our results for a low sedimentation, continental margin environment support this important role of CFA for global reactive P burial.

8. Conclusions

The results of solid phase P speciation for sediments from two stations on the North Atlantic continental platform Goban Spur indicate that authigenic carbonate fluorapatite (CFA) may be forming in the sediment at the expense of Fe-bound P.

Application of a diagenetic phosphorus model to solid phase P (organic P, Fe-bound P and authigenic P) and pore water HPO_4^{2-} profiles, indicates that CFA formation can account for the increase of authigenic P with depth at one station. The model results demonstrate that an intense cycling of P between Fe-bound P and pore water HPO_4^{2-} can be responsible for elevated pore water HPO_4^{2-} concentrations below the redox-interface, thus creating conditions beneficial for CFA formation. This cycle is driven by bioturbation through downward transport of in-situ formed Fe-bound P and refueled by sorption of HPO_4^{2-} released from organic matter to Fe oxides. This mechanism, in which Fe-bound P plays a key role, acting as an intermediate between organic P and CFA, may be of particular importance in marine sediments with low sedimentation rates where organic matter decomposition takes place close to the sediment-water interface. In these environments, CFA may then become an important sink for P.

Acknowledgments. We thank Henko de Stigter and Tjeerd van Weering for supplying data on sedimentation and bioturbation rates at the studied stations. Johan den Das, Hans Malschaert, Annette van Koutrik and Jan van Ooijen performed part of the analyses. Thanks are due to the crew of RV *Pelagia* and Marlen Dekker for their assistance during the cruise. This research is part of the OMEX (Ocean Margin Exchange) program funded by EC Mast II (contract nr. MAS2-CT93-0069). This is publication no. 3057 of the Netherlands Institute for Sea Research (NIOZ).

APPENDIX

The differential equations for each P reservoir in the (I) oxidized surface zone ($0 \leq x \leq L_1$), (II) reduced sediment zone with bioturbation ($L_1 < x \leq L_2$) and (III) reduced sediment zone without bioturbation ($x > L_2$), with ϑ as given in Eq. (1) and all other symbols as listed in Tables 2 and 3, are as follows:

Pore water HPO_4^{2-} (C)

$$\frac{\partial C_I}{\partial t} = [D_b + D_s]\frac{\partial^2 C_\mathrm{I}}{\partial x^2} - \omega\frac{\partial C_I}{\partial x} + k_g\vartheta(G_I - G_\infty) - k_s(C_I - C_s) = 0 \qquad \text{(A1)}$$

$$\frac{\partial C_\mathrm{II}}{\partial t} = [D_b + D_s]\frac{\partial^2 C_\mathrm{II}}{\partial x^2} - \omega\frac{\partial C_\mathrm{II}}{\partial x} + k_g\vartheta(G_\mathrm{II} - G_\infty) - k_a(C_\mathrm{II} - C_a) + k_m\vartheta(M_\mathrm{II} - M_\infty) = 0 \qquad \text{(A2)}$$

$$\frac{\partial C_\mathrm{III}}{\partial t} = D_s\frac{\partial^2 C_\mathrm{III}}{\partial x^2} - \omega\frac{\partial C_\mathrm{III}}{\partial x} + k_g\vartheta(G_\mathrm{III} - G_\infty) - k_a(C_\mathrm{III} - C_a) + k_m\vartheta(M_\mathrm{III} - M_\infty) = 0 \qquad \text{(A3)}$$

Organic P (G)

$$\frac{\partial G_{\mathrm{I}}}{\partial t} = D_b \frac{\partial^2 G_{\mathrm{I}}}{\partial x^2} - \omega \frac{\partial G_{\mathrm{I}}}{\partial x} - k_g(G_{\mathrm{I}} - G_\infty) = 0 \tag{A4}$$

$$\frac{\partial G_{\mathrm{II}}}{\partial t} = D_b \frac{\partial^2 G_{\mathrm{II}}}{\partial x^2} - \omega \frac{\partial G_{\mathrm{II}}}{\partial x} - k_g(G_{\mathrm{II}} - G_\infty) = 0 \tag{A5}$$

$$\frac{\partial G_{\mathrm{III}}}{\partial t} = -\omega \frac{\partial G_{\mathrm{III}}}{\partial x} - k_g(G_{\mathrm{III}} - G_\infty) = 0 \tag{A6}$$

Fe-bound P (M)

$$\frac{\partial M_{\mathrm{I}}}{\partial t} = D_b \frac{\partial^2 M_{\mathrm{I}}}{\partial x^2} - \omega \frac{\partial M_I}{\partial x} + \frac{k_s}{\vartheta}(C_{\mathrm{I}} - C_s) = 0 \tag{A7}$$

$$\frac{\partial M_{\mathrm{II}}}{\partial t} = D_b \frac{\partial^2 M_{\mathrm{II}}}{\partial x^2} - \omega \frac{\partial M_{\mathrm{II}}}{\partial x} - k_m(M_{\mathrm{II}} - M_\infty) = 0 \tag{A8}$$

$$\frac{\partial M_{\mathrm{III}}}{\partial t} = -\omega \frac{\partial M_{\mathrm{III}}}{\partial x} - k_m(M_{\mathrm{III}} - M_\infty) = 0 \tag{A9}$$

Authigenic P (A)

$$\frac{\partial A_{\mathrm{I}}}{\partial t} = D_b \frac{\partial^2 A_{\mathrm{I}}}{\partial x^2} - \omega \frac{\partial A_{\mathrm{I}}}{\partial x} = 0 \tag{A10}$$

$$\frac{\partial A_{\mathrm{II}}}{\partial t} = D_b \frac{\partial^2 A_{\mathrm{II}}}{\partial x^2} - \omega \frac{\partial A_{\mathrm{II}}}{\partial x} + \frac{k_a}{\vartheta}(C_{\mathrm{II}} - C_a) = 0 \tag{A11}$$

$$\frac{\partial A_{\mathrm{III}}}{\partial t} = -\omega \frac{\partial A_{\mathrm{III}}}{\partial x} + \frac{k_a}{\vartheta}(C_{\mathrm{III}} - C_a) = 0 \tag{A12}$$

The boundary conditions used to solve the Eqs. (A1) to (A12) are:
at $x = 0$

$$C_{\mathrm{I}} = C_o \tag{A13}$$

$$J_{G_{x=0}} = -\phi\vartheta\left[D_b \frac{\partial G}{\partial x} - \omega G\right]_{x=0} \tag{A14}$$

$$J_{M_{x=0}} = -\phi\vartheta\left[D_b \frac{\partial M}{\partial x} - \omega M\right]_{x=0} \tag{A15}$$

$$J_{A_{x=0}} = -\phi\vartheta\left[D_b \frac{\partial A}{\partial x} - \omega A\right]_{x=0} \tag{A16}$$

at $x = L_1$

$$C_{\mathrm{I}} = C_{\mathrm{II}} \tag{A17}$$

$$G_{\mathrm{I}} = G_{\mathrm{II}} \tag{A18}$$

$$M_{\mathrm{I}} = M_{\mathrm{II}} \tag{A19}$$

$$A_{\mathrm{I}} = A_{\mathrm{II}} \tag{A20}$$

$$[D_b + D_s]\frac{\partial C_{\mathrm{I}}}{\partial x} - \omega C_{\mathrm{I}} = [D_b + D_s]\frac{\partial C_{\mathrm{II}}}{\partial x} - \omega C_{\mathrm{II}} \tag{A21}$$

$$D_b\frac{\partial G_{\mathrm{I}}}{\partial x} - \omega G_{\mathrm{I}} = D_b\frac{\partial G_{\mathrm{II}}}{\partial x} - \omega G_{\mathrm{II}} \tag{A22}$$

$$D_b\frac{\partial M_{\mathrm{I}}}{\partial x} - \omega M_{\mathrm{I}} = D_b\frac{\partial M_{\mathrm{II}}}{\partial x} - \omega M_{\mathrm{II}} \tag{A23}$$

$$D_b\frac{\partial A_{\mathrm{I}}}{\partial x} - \omega A_{\mathrm{I}} = D_b\frac{\partial A_{\mathrm{II}}}{\partial x} - \omega A_{\mathrm{II}} \tag{A24}$$

at $x = L_2$

$$C_{\mathrm{II}} = C_{\mathrm{III}} \tag{A25}$$

$$G_{\mathrm{II}} = G_{\mathrm{III}} \tag{A26}$$

$$M_{\mathrm{II}} = M_{\mathrm{III}} \tag{A27}$$

$$A_{\mathrm{II}} = A_{\mathrm{III}} \tag{A28}$$

$$[D_b + D_s]\frac{\partial C_{\mathrm{II}}}{\partial x} - \omega C_{\mathrm{II}} = D_s\frac{\partial C_{\mathrm{III}}}{\partial x} - \omega C_{\mathrm{III}} \tag{A29}$$

$$D_b\frac{\partial G_{\mathrm{II}}}{\partial x} - \omega G_{\mathrm{II}} = -\omega G_{\mathrm{III}} \tag{A30}$$

$$D_b\frac{\partial M_{\mathrm{II}}}{\partial x} - \omega M_{\mathrm{II}} = -\omega M_{\mathrm{III}} \tag{A31}$$

$$D_b\frac{\partial A_{\mathrm{II}}}{\partial x} - \omega A_{\mathrm{II}} = -\omega A_{\mathrm{III}} \tag{A32}$$

when $x \rightarrow \infty$

$$C_{\mathrm{III}} \rightarrow C_a \tag{A33}$$

$$G_{\mathrm{III}} \rightarrow G_\infty \tag{A34}$$

$$M_{\mathrm{III}} \rightarrow M_\infty \tag{A35}$$

The solutions to the equations and the Excel worksheet containing the model can be obtained from the first author upon request.

REFERENCES

Aller, R. C. 1990. Bioturbation and manganese cycling in hemipelagic sediments. Phil. Trans. R. Soc. London. A., *331,* 51–68.

Aspila, K. I., H. Agemian and A. S. Y. Chau. 1976. A semi-automated method for the determination of inorganic, organic and total phosphate in sediments. Analyst, *101,* 187–197.

Atlas, E. and R. M. Pytkowicz. 1977. Solubility behavior of apatites in seawater. Limnol. Oceanogr., *22,* 290–300.

Berner, R. A. 1980. Early Diagenesis: A Theoretical Approach, Princeton University Press, Princeton, NJ, 241 pp.

Berner, R. A., K. C. Ruttenberg, E. D. Ingall, and J.-L. Rao. 1993. The nature of phosphorus burial in modern marine sediments, *in* Interactions of C, N, P, and S Biogeochemical Cycles and Global Change, R. Wollast, F. T. Mackenzie and L. Chou, eds., Springer-Verlag, NATO ASI Series *14,* 521 pp.

Bray, J. T., O. P. Bricker and B. N. Troup. 1973. Phosphate in interstitial waters of anoxic sediments: oxidation effects during sampling procedures. Science, *180,* 1362–1364.

Brewer, P. G. and D. W. Spencer. 1971. Colorimetric determination of manganese in anoxic waters. Limnol. Oceanogr., *16,* 107–110.

Broecker, W. S. and T.-H. Peng. 1982. Tracers in the Sea, Eldigio Press, Palisades, NY, 690 pp.

Burdige, D. J. and J. M. Gieskes. 1983. A pore water/solid phase diagenetic model for manganese in marine sediments. Am. J. Sci., *283,* 29–47.

Canfield, D. E., R. Raiswell and S. Bottrell. 1992. The reactivity of sedimentary iron minerals toward sulfide. Am. J. Sci., *292,* 659–683.

Canfield, D. E., B. Thamdrup and J. W. Hansen. 1993. The anaerobic degradation of organic matter in Danish coastal sediments: iron reduction, manganese reduction, and sulfate reduction. Geochim. Cosmochim. Acta, *57,* 3867–3883.

Draper, N. R. and H. Smith. 1967. Applied Regression Analysis, John Wiley, 407 pp.

Flach, E. and C. Heip. 1996. Vertical distribution within the sediment of macrozoobenthos along the continental slope in the Goban Spur area (NE Atlantic). Mar. Ecol. Prog. Ser., (in press).

Froelich, P. N. 1988. Kinetic control of dissolved phosphate in natural rivers and estuaries: a primer on the phosphate buffer mechanism. Limnol. Oceanogr., *33,* 649–668.

Froelich, P. N., M. A. Arthur, W. C. Burnett, M. Deakin, V. Hensley, R. Jahnke, L. Kaul, K.-H. Kim, K. Roe, A. Soutar and C. Vathakanon. 1988. Early diagenesis of organic matter in Peru continental margin sediments: phosphorite precipitation. Mar. Geol., *80,* 309–343.

Gerke, J. and R. Hermann. 1992. Adsorption of orthophosphate to humic-Fe-complexes and to amorphous Fe-oxide. Z. Planzenernähr. Bodenk., *155,* 233–236.

Heggie, D. T., D. Kahn and K. Fischer. 1986. Trace metals in metalliferous sediments. MANOP Site M: interfacial pore water profiles. Earth Planet. Sci. Lett., *80,* 106–116.

Heggie, D. T., G. W. Skyring, G. W. O'Brein, C. Reimers, A. Herczeg, D. J. W. Moriarty, W. C. Burnett, A. R. Milnes. 1990. Organic carbon cycling and modern phosphorite formation on the East Australian continental margin: An overview, *in* Phosphorite research and development, G. J. Notholt and I. Jarvis, eds., Geol. Soc. Spec. Publ., *52,* 87–117.

Helder, W. and R. P. T. De Vries. 1979. An automatic phenol-hypochlorite method for the determination of ammonia in sea- and brackish waters. Neth. J. Sea. Res., *13,* 154–160.

Howarth, R. W., H. Jensen, R. Marino and H. Postma. 1995. Transport to and processing of phosphorus in near-shore and oceanic waters, *in* Phosphorus in the Global Environment, H. Tiessen, ed., John Wiley, SCOPE 54, 462 pp.

Ingall, E. D. and P. Van Cappellen. 1990. Relation between sedimentation rate and burial of organic phosphorus and organic carbon in marine sediments. Geochim. Cosmochim. Acta, *54,* 373–386.

Jahnke, R. A., S. R. Emerson, K. K. Roe and W. C. Burnett. 1983. The present day formation of apatite in Mexican continental margin sediments. Geochim. Cosmochim. Acta, *47,* 259–266.

Jensen, H. S. and B. Thamdrup. 1993. Iron-bound phosphorus in marine sediments as measured by the bicarbonate-dithionite extraction. Hydrobiologia, *253,* 47–59.

Jørgensen, B. B. 1977. Bacterial sulfate reduction within reduced microniches of oxidized marine sediments. Mar. Biol., *41,* 7–17.

Kalhorn, S. and S. Emerson. 1984. The oxidation state of manganese in surface sediments of the deep sea. Geochim. Cosmochim. Acta, *48,* 897–902.

Krom, M. D. and R. A. Berner. 1980. The diffusion coefficient of sulfate, ammonium and phosphate ions in anoxic marine sediments. Limnol. Oceanogr., *25,* 327–337.

Lovley, D. R. 1991. Dissimilatory Fe(III) and Mn(IV) reduction. Microbiol. Rev., *55,* 259–287.

Lucotte, M., A. Mucci and A. Hillairemarcel. 1994. Early diagenetic processes in deep Labrador Sea sediments: reactive and nonreactive iron and phosphorus. Can. J. Earth Sci., *31,* 14–27.

Martens, C. S., R. A. Berner and J. K. Rosenfeld. 1978. Interstitial water chemistry of anoxic Long Island Sound sediments. 2. Nutrient regeneration and phosphate removal. Limnol. Oceanogr., *23,* 605–617.

Pettijohn, F. J., P. E. Potter and R. Siever. 1972. Sand and Sandstone. Springer, NY, 618 pp.

Reeburgh, W. S. 1967. An improved interstitial water sampler. Limnol. Oceanogr., *12,* 163–170.

Ruttenberg, K. C. 1992. Development of a sequential extraction method for different forms of phosphorus in marine sediments. Limnol. Oceanogr., *37,* 1460–1482.

—— 1993. Reassessment of the oceanic residence time of phosphorus. Chem. Geol., *107,* 405–409.

Ruttenberg, K. C. and R. A. Berner. 1993. Authigenic apatite formation and burial in sediments from non-upwelling, continental margin environments. Geochim. Cosmochim. Acta, *57,* 991–1007.

Schwertmann, U. 1991. Solubility and dissolution of iron oxides. Plant and Soil, *130,* 1–25.

Sherwood, B. A., S. L. Sager and H. D. Holland. 1987. Phosphorus in foraminiferal sediments from North Atlantic Ridge cores and in pure limestones. Geochim. Cosmochim. Acta, *51,* 1861–1866.

Slomp, C. P., S. J. Van der Gaast and W. Van Raaphorst. 1996. Phosphorus binding by poorly crystalline iron oxides in North Sea sediments. Mar. Chem., *52,* 55–73.

Slomp, C. P. and W. Van Raaphorst. 1993. Phosphate adsorption in oxidized marine sediments. Chem. Geol., *107,* 477–480.

Stookey, L. L. 1970. Ferrozine—A new spectrophotometric reagent for iron. Analyt. Chem., *42,* 779–781.

Strickland, T. R. and J. D. Parsons. 1972. A Practical Handbook of Seawater Analysis, 2nd. ed., Bull. Fish. Res. Bd. Can., *167,* 1–311.

Stumm, W. and B. Sulzberger. 1992. The cycling of iron in natural environments: Considerations based on laboratory studies of heterogeneous redox processes. Geochim. Cosmochim. Acta, *56,* 3233–3257.

Sundby, B., C. Gobeil, N. Silverberg and A. Mucci. 1992. The phosphorus cycle in coastal marine sediments. Limnol. Oceanogr., *37,* 1129–1145.

Tromp, T. K., P. Van Cappellen and R. M. Key. 1995. A global model for the early diagenesis of organic carbon and organic phosphorus in marine sediments. Geochim. Cosmochim. Acta, *59,* 1259–1284.

Van Cappellen, P. and R. A. Berner. 1988. A mathematical model for the early diagenesis of phosphorus and fluorine in marine sediments: apatite precipitation. Am. J. Sci., *288,* 289–333.

Van Raaphorst, W., P. Ruardij and A. G. Brinkman. 1988. The assessment of benthic phosphorus regeneration in an estuarine ecosystem model. Neth. J. Sea Res., *22,* 23–36.

Van Raaphorst, W., H. T. Kloosterhuis, A. Cramer and K. J. M. Bakker. 1990. Nutrient early diagenesis in the sandy sediments of the Dogger Bank area: pore water results. Neth. J. Sea Res., *26,* 25–52.

Van Raaphorst, W. and H. T. Kloosterhuis. 1994. Phosphate sorption in superficial intertidal sediments. Mar. Chem., *48,* 1–16.

Verardo, D. J., P. N. Froelich and A. McIntyre. 1990. Determination of organic carbon and nitrogen in sediments using the Carlo Erba Na-1500 analyzer. Deep-Sea Res., *37,* 157–165.

Received: *18 January, 1996;* revised: *30 July, 1996.*